https://dx.doi.org/10.1016/j.jmps.2022.104919

A generalized solution to the combo-crack problem—II. Remote load

Haimin Yao*, Chong Zhang
Department of Mechanical Engineering, The Hong Kong Polytechnic University, Hung Hom, Kowloon, Hong Kong SAR, China

*To whom correspondence should be addressed, E-Mail: mmhyao@polyu.edu.hk (H. Yao)

Abstract

In Part I, we studied the combo-crack problem, which contains an interior penny-shaped crack (PSC) and a coplanar and concentric externally circular crack (ECC), under pressure load applied to the surface of the interior PSC. In fact, a more common type of loading experienced by cracked media might be remote tension normal to the crack plane. For a combo crack under remote tension, a reliable solution remains deficient. In this paper, we extend our discussion to the case of remote tension in the theoretical framework developed in Part I. We for the first time formulate the concerned mixed boundary value problem into a single inhomogeneous Fredholm integral equation, which is then solved numerically with a *Gauss-Lobatto* quadrature-based algorithm. The normal stress in the ligament (bonded) region on the plane of the crack, the stress intensity factors at the tips of PSC and ECC, and the critical force load for trigging crack propagation are determined, showing an excellent agreement with the finite element results. Our work provides a high-precision numerical solution to the combo-crack problem for the most basic loading case. The obtained results should be of general value to the resolution of a bunch of fracture and adhesion problems in combo-crack configuration in engineering and deserve to be absorbed into the updated handbook for basic crack problems.

Keywords:

Fredholm integral equation; Stress intensity factor; *Gauss-Lobatto* quadrature; Annular contact problem; Remote load

1. Introduction

A combo crack is a dual-crack configuration containing an interior penny-shaped crack (PSC) and a coplanar concentric externally circular crack (ECC). The elasticity problem of a combo crack under axisymmetric load is mathematically equivalent to the frictionless contact problem between an elastic half-space and a rigid annular flat punch. Both problems can be formulated into a triple mixed boundary value problem. Up to now, no closed-form solution has been found for such kind of mixed boundary value problem. In Part I (Yao and Zhang, 2022), we developed a theoretical framework to solve the combo-crack problem upon the axisymmetric pressure load applied to the surfaces of the interior PSC. Our solutions to the stress intensity factors (SIFs) at both crack tips, albeit not in closed form, exhibit higher precision in comparison to the previous ones. Nevertheless, a more common loading type encountered by a combo crack, or an equivalent annular adhesion joint, might be the remote axisymmetric load normal to the crack plane, as shown in Figure 1a and Figure 1b respectively. Although such a basic loading case has been considered many times using various mathematical techniques(Gladwell and Gupta, 1979; Shibuya et al., 1974) and some investigations even extended to the sophisticated cases involving non-axisymmetric loads (Fabrikant, 1991; Yong and Hanson, 1994) and nonhomogeneous media (Shield and Bogy, 1989), it is surprising to note that we still do not have a reliable solution to the combo-crack problem even under remote axisymmetric load. For instance, in the most recent attempt at the combo-crack problem (Yong and Hanson, 1994), Yong and Hanson used the Boussinesq solution for point normal loading on an elastic half-space as the Green's function to establish a two-dimensional integral equation about the unknown normal stress (σ_{zz}) in the annular ligament region on the crack plane. By taking the unknown normal stress as a power series, they numerically solved the equation and obtained the approximate solution to the normal stress, based on which the SIFs at both crack tips were determined. Regretfully, in their definition of SIFs, a factor of $\sqrt{\pi}$ is missing as compared to the conventional definition $K_{\mathrm{I}} = \lim_{\rho\to 0}\sqrt{2\pi\rho}\,\sigma_{zz}(\rho)$, where ρ stands for the distance to the crack tip. Unfortunately, such a flawed solution was absorbed by a handbook on stress intensity factors (Murakami, 1992). The spread and applications of such problematic results in engineering might cause unpredictable negative consequences. Even though the missing factor $\sqrt{\pi}$ gets supplemented in their solution, their SIFs still exhibit certain error especially in the extreme cases when the interior PSC is either distant or very close to the ECC. This is essentially attributed to the unavoidable truncation

error of the power series assumed for the unknown normal stress. To address these issues and find a reliable solution to the combo-crack problem under remote load, in this paper we reattempt the problem with an alternative approach we developed recently in Part I. Based on the well-known Hankel transform-based representations of the solution to the axisymmetric elasticity problems, we first formulate the concerned mixed boundary value problem into a pair of simultaneous Fredholm integral equations, which are tactically merged into a single inhomogeneous Fredholm integral equation. *Gauss-Lobatto* quadrature-based approach is then applied to solve the inhomogeneous integral equation numerically, followed by the determination of the normal stress, SIFs, and force load. Our numerical solution shows an excellent agreement with the finite element results and higher precision in comparison with the previous power series-based solution. The remainder of this paper is structured as follows. In Section 2, we theoretically formulate the problem into an inhomogeneous integral equation about one unknown function, whose solution could directly lead to the resolution of the problem. In Section 3 we develop a numerical algorithm to solve the integral equation after converting it into a normalized form, followed by the determination of the solution to the normal stress in the ligament region, SIFs at the PSC and ECC, and the net force. In Section 4, the numerical solutions to these quantities and their dependences on the sizes of the PSC and ECC are illustrated, followed by the extended discussion on the propagating behaviour of a combo crack under combined load of pressure on the PSC surface and the remote force load. Finally, the whole paper is concluded in Section 5.

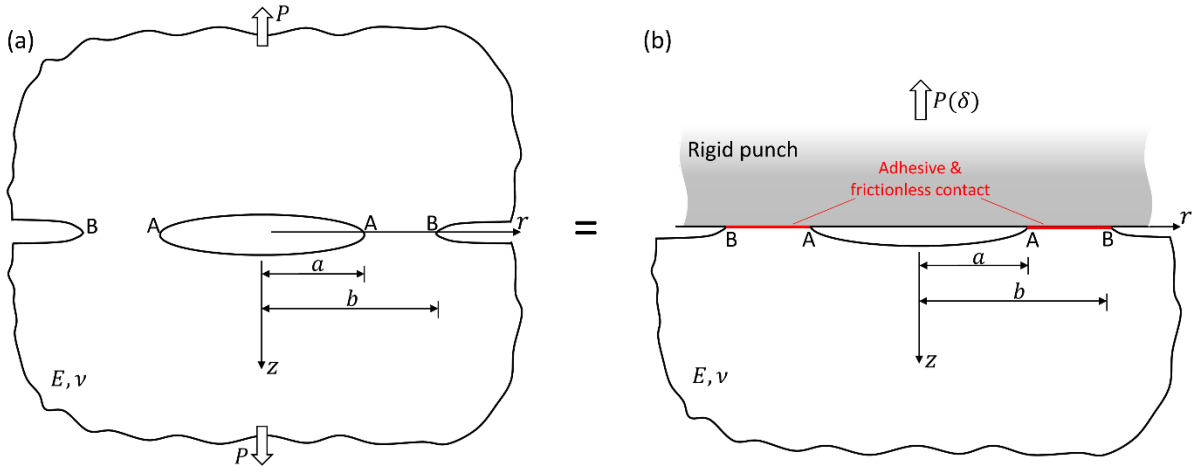

Fig. 1. (a) Cross-sectional illustrations of the axisymmetric combo-crack problem which contains an externally circular crack (ECC) of radius b embracing a coplanar concentric penny-shaped crack (PSC) of radius a. A remote uniaxial force load is applied along the axis of symmetry. (b) Cross-sectional illustration of the equivalent annular contact problem of an elastic half-space in adhesive and frictionless contact with a rigid flat punch via an annular

region ($a < r < b$). A uniaxial tensile load is applied to the rigid punch along the axis of symmetry. The displacement of the half-space in the distance ($z \to \infty$) is constrained.

2. Theoretical formulation and solutions

Consider a crack combo under remote tensile load (see Fig. 1a) or equivalently an elastic half-space in adhesive and frictionless contact with a rigid punch through an annular region ($a < r < b$) under tensile load (see Fig. 1b). Using the Hankel transform-based representations of the solution to axisymmetric half-space problems, one can express the above mixed boundary value problems into a set of triple integral equations about an unknown function $A(\xi)$ (Yao and Zhang, 2022)

$$\int_0^\infty A(\xi) J_0(\xi r)\, d\xi = 0, \quad (0 \le r \le a) \tag{1a}$$

$$\int_0^\infty \xi^{-1} A(\xi) J_0(\xi r)\, d\xi = -\frac{E^* \delta}{2}, \quad (a < r < b) \tag{1b}$$

$$\int_0^\infty A(\xi) J_0(\xi r)\, d\xi = 0, \quad (b \le r < \infty) \tag{1c}$$

where $J_0(\cdot)$ is the 0-th order Bessel function of the first kind, E^* is the plane-strain modulus of the half-space, δ is the normal displacement load applied to the annular ligament (bonded) region ($a < r < b$). The solution to $A(\xi)$ is given by (Cooke, 1963)

$$A(\xi) = \xi^2 \left\{ \int_0^a r f_1(r) J_0(\xi r)\, dr - \int_a^b \frac{r E^* \delta}{2} J_0(\xi r) dr + \int_b^\infty r f_2(r) J_0(\xi r)\, dr \right\} \tag{2}$$

where $f_1(r)$ and $f_2(r)$ represent the 0-th order Hankel transform of $\xi^{-2} A(\xi)$ in the domains of $0 \le r \le a$ and $b \le r < \infty$, respectively. That is, they are related to the normal displacement $u_z(r)$ on the PSC and ECC surfaces through

$$\frac{E^*}{2} u_z(r) = \int_0^\infty \xi^{-1} A(\xi) J_0(\xi r)\, d\xi \equiv \begin{cases} f_1(r), & (0 \le r \le a) \\ f_2(r), & (b \le r < \infty) \end{cases} \tag{3}$$

Functions $f_1(r)$ and $f_2(r)$ are correlated with each other through a pair of simultaneous integral equations as follows (Cooke, 1963)

$$f_1(r) = \frac{2}{\pi} \left(a^2 - r^2\right)^{1/2} \left[-\frac{E^* \delta}{2} \int_a^b \frac{t dt}{(t^2 - r^2)\left(t^2 - a^2\right)^{1/2}} + \int_b^\infty \frac{t f_2(t)\, dt}{(t^2 - r^2)\left(t^2 - a^2\right)^{1/2}} \right], (0 \le r \le a) \tag{4a}$$

$$f_2(r)=\frac{2}{\pi}\left(r^2-b^2\right)^{1/2}\left[\int_0^a \frac{tf_1(t)dt}{\left(r^2-t^2\right)\left(b^2-t^2\right)^{1/2}}-\frac{E^*\delta}{2}\int_a^b \frac{tdt}{\left(r^2-t^2\right)\left(b^2-t^2\right)^{1/2}}\right],\left(b\le r<\infty\right) \quad (4b)$$

The integrations in the above equations can be implemented as

$$\int_a^b \frac{tdt}{(t^2-r^2)\left(t^2-a^2\right)^{1/2}}=\frac{1}{\left(a^2-r^2\right)^{1/2}}\arctan\left(\frac{b^2-a^2}{a^2-r^2}\right)^{1/2},\ \left(0\le r\le a\right)$$

$$\int_a^b \frac{tdt}{\left(r^2-t^2\right)\left(b^2-t^2\right)^{1/2}}=\frac{1}{\left(r^2-b^2\right)^{1/2}}\arctan\left(\frac{b^2-a^2}{r^2-b^2}\right)^{1/2},\ \left(b\le r<\infty\right)$$

Eqs. (4a) and (4b) thus can be rewritten as

$$f_1(r)=p_1(r)+\frac{2}{\pi}\int_b^\infty \frac{t\left(a^2-r^2\right)^{1/2}f_2(t)dt}{(t^2-r^2)\left(t^2-a^2\right)^{1/2}},\ \left(0\le r\le a\right) \quad (5a)$$

$$f_2(r)=p_2(r)+\frac{2}{\pi}\int_0^a \frac{t\left(r^2-b^2\right)^{1/2}f_1(t)dt}{\left(r^2-t^2\right)\left(b^2-t^2\right)^{1/2}},\ \left(b\le r<\infty\right) \quad (5b)$$

where

$$p_1(r)\equiv-\frac{E^*\delta}{\pi}\arctan\left(\frac{b^2-a^2}{a^2-r^2}\right)^{1/2},\left(0\le r\le a\right) \quad (5c)$$

$$p_2(r)\equiv-\frac{E^*\delta}{\pi}\arctan\left(\frac{b^2-a^2}{r^2-b^2}\right)^{1/2},\ \left(b\le r<\infty\right) \quad (5d)$$

From Eqs. (5a) and (5b), it can be readily verified that $f_1(a)=f_2(b)=-\frac{E^*\delta}{2}$, implying that the continuity condition of displacement $u_z(r)$ at the edges of the annular bonded region is satisfied.

Following the approach developed by (Selvadurai and Singh, 1987), we introduce two additional auxiliary functions $F_1(r)$ and $F_2(r)$ through

$$F_1(r)=\frac{d}{dr}\int_r^a \frac{tf_1(t)dt}{\left(t^2-r^2\right)^{1/2}},\ \left(0\le r\le a\right) \quad (6a)$$

131 $$F_2(r)=\frac{d}{dr}\int_b^r \frac{tf_2(t)dt}{\left(r^2-t^2\right)^{1/2}},\ \left(b\le r<\infty\right) \tag{6b}$$

132 The solutions to the above two Abel integral equations in turn express the functions $f_1(\cdot)$ and
133 $f_2(\cdot)$ in terms of $F_1(\cdot)$ and $F_2(\cdot)$ as

134 $$f_1(t)=-\frac{2}{\pi}\int_t^a \frac{F_1(s)ds}{\left(s^2-t^2\right)^{1/2}},\ \left(0\le r\le a\right) \tag{7a}$$

135 $$f_2(t)=\frac{2}{\pi}\int_b^t \frac{F_2(s)ds}{\left(t^2-s^2\right)^{1/2}},\ \left(b\le r<\infty\right) \tag{7b}$$

136 Inserting Eqs. (5a) into (6a), and Eq. (5b) into (6b) and then applying Eqs. (7a), (7b), (5c), and
137 (5d), we obtain the following simultaneous Fredholm integral equations about the unknown
138 functions $F_1(s)$ and $F_2(s)$ as (see **Appendix A**)

139 $$F_1(s)+\frac{2s}{\pi}\int_b^\infty \frac{F_2(u)du}{\left(u^2-s^2\right)}=\frac{E^*\delta}{2}\left[\frac{s}{\left(a^2-s^2\right)^{1/2}}-\frac{s}{\left(b^2-s^2\right)^{1/2}}\right],\ \left(0\le s\le a\right) \tag{8a}$$

140 $$F_2(s)+\frac{2}{\pi}\int_0^a \frac{uF_1(u)du}{\left(s^2-u^2\right)}=\frac{E^*\delta}{2}\left[\frac{s}{\left(s^2-a^2\right)^{1/2}}-\frac{s}{\left(s^2-b^2\right)^{1/2}}\right],\left(b\le s<\infty\right) \tag{8b}$$

141 In view of the constructive feature of Eqs. (8a) and (8b), without loss of generality, we express
142 $F_1(s)$ and $F_2(s)$ as

143 $$F_1(s)=\frac{E^*\delta}{2}\frac{s}{\left(a^2-s^2\right)^{1/2}}+F_1^*(s),\ \left(0\le s\le a\right) \tag{9a}$$

144 $$F_2(s)=-\frac{E^*\delta}{2}\frac{s}{\left(s^2-b^2\right)^{1/2}}+F_2^*(s),\ \left(b\le s<\infty\right) \tag{9b}$$

145 where $F_1^*(s)$ and $F_2^*(s)$ are two unknown functions to be determined. Inserting Eq. (9a) and
146 Eq. (9b) into Eq. (8a) and Eq. (8b) respectively gives rise to a pair of simplified simultaneous
147 Fredholm integral equations about the unknown functions $F_1^*(s)$ and $F_2^*(s)$

148 $$F_1^*(s)+\frac{2s}{\pi}\int_b^\infty \frac{F_2^*(u)du}{\left(u^2-s^2\right)}=0,\ \left(0\le s\le a\right) \tag{10a}$$

$$F_2^*(s)+\frac{2}{\pi}\int_0^a \frac{uF_1^*(u)\,du}{\left(s^2-u^2\right)}=\frac{E^*\delta}{2},\ (b\le s<\infty) \tag{10b}$$

In the derivation of Eqs. (10a) and (10b) above, the following two relationships have been adopted

$$\int_b^\infty \frac{udu}{\left(u^2-b^2\right)^{1/2}\left(u^2-s^2\right)}=\frac{\pi}{2\left(b^2-s^2\right)^{1/2}},\ (0\le s\le a<b)$$

$$\int_0^a \frac{u^2du}{\left(a^2-u^2\right)^{1/2}\left(s^2-u^2\right)}=\frac{\pi}{2}\left[\frac{s}{\left(s^2-a^2\right)^{1/2}}-1\right],\ (a<b\le s)$$

Substituting Eq. (10b) into Eq. (10a) to eliminate $F_2^*(s)$, we obtain

$$F_1^*(s)+\frac{2}{\pi^2}\int_0^a Q_1(u,s)F_1^*(u)\,du=\frac{E^*\delta}{2\pi}\ln\frac{b-s}{b+s},\ (0\le s\le a) \tag{11a}$$

where

$$Q_1(u,s)\equiv\left(u\ln\frac{b+s}{b-s}-s\ln\frac{b+u}{b-u}\right)\frac{1}{\left(u^2-s^2\right)},\ (0\le s\le a) \tag{11b}$$

is the symmetric kernel function. It can be demonstrated that $\lim_{u\to s}Q_1(u,s)=\frac{1}{2s}\ln\frac{b+s}{b-s}+\frac{b}{s^2-b^2}$, which approaches 0 as $s\to 0$. Eq. (11a) is a typical inhomogeneous Fredholm integral equation of the unknown function $F_1^*(s)$. Finding its analytical solution remains challenging unless in the limiting case of $a/b\to 0$. A numerical approach can be adopted to solve it, as will be elaborated in Section 3. Once the numerical solution to $F_1^*(s)$ is obtained, $F_2^*(s)$ can be easily determined through Eq. (10b) via numerical integration.

The normal stress σ_{zz} in the annular ligament (bonded) region ($a<r<b$) can also be given in terms of functions of $F_1^*(s)$ and $F_2^*(s)$ as (see **Appendix B**)

$$\sigma_{zz}(r)=-\frac{2}{\pi}\int_0^a \frac{sF_1^*(s)\,ds}{\left(r^2-s^2\right)^{3/2}}+\frac{2}{\pi}\int_b^\infty \frac{sF_2^*(s)}{\left(s^2-r^2\right)^{3/2}}ds,\ (a<r<b) \tag{12}$$

Considering the correlations between functions $F_1^*(s)$ and $F_2^*(s)$ given by Eqs. (10a) and (10b), the normal stress σ_{zz} above can be further expressed as a function of $F_1^*(s)$ and its derivative $F_1^{*\prime}(s)$ (see **Appendix B**):

$$\sigma_{zz}(r)=\frac{4}{\pi^2}\left[\begin{array}{l}-\arctan\left(\dfrac{b^2-r^2}{r^2-a^2}\right)^{1/2}\dfrac{F_1^*(a)}{\left(r^2-a^2\right)^{1/2}}+\dfrac{\pi F_2^*(b)}{2\left(b^2-r^2\right)^{1/2}}\\ +\displaystyle\int_0^a\frac{F_1^{*\prime}(u)}{\left(r^2-u^2\right)^{1/2}}\arctan\left(\frac{b^2-r^2}{r^2-u^2}\right)^{1/2}du\end{array}\right],\ (a<r<b) \tag{13a}$$

where

$$F_2^*(b)=\frac{E^*\delta}{2}+\frac{1}{\pi}\left[F_1^*(a)\ln\left(b^2-a^2\right)-\int_0^a\ln\left(b^2-u^2\right)F_1^{*\prime}(u)\,du\right] \tag{13b}$$

As expected, the normal stress σ_{zz} given by Eq. (13a) exhibits square-root singularity at the tips of the PSC (point A) and ECC (point B) with $r=a$ and $r=b$, respectively. The corresponding SIFs (mode I) are given by

$$K_{\mathrm{A}}=\lim_{r\to a^+}\left[2\pi(r-a)\right]^{1/2}\sigma_{zz}(r)=-\frac{2}{\sqrt{a\pi}}F_1^*(a) \tag{14a}$$

$$K_{\mathrm{B}}=\lim_{r\to b^-}\left[2\pi(b-r)\right]^{1/2}\sigma_{zz}(r)=\frac{2}{\sqrt{b\pi}}F_2^*(b) \tag{14b}$$

The net force P corresponding to the given displacement δ, which is equal to the integration of the stress σ_{zz} over the whole annular bonded region ($a<r<b$), is given by (see **Appendix B**)

$$P=2\pi\int_a^b\sigma_{zz}(r)\,r\,dr=2E^*\delta\left(b^2-a^2\right)^{1/2}-\frac{8}{\pi}\int_0^a\arctan\left(\frac{b^2-a^2}{a^2-u^2}\right)^{1/2}\frac{uF_1^*(u)}{\left(a^2-u^2\right)^{1/2}}du \tag{15}$$

Based on the numerical solution to $F_1^*(s)$ resolved from Eq. (11a), the normal stress σ_{zz}, SIFs K_{A}, K_{B}, and net force P can be determined readily through Eqs. (13-15) by numerical integration. In the following, a numerical algorithm will be developed to solve Eq. (11a) for the unknown function $F_1^*(s)$, followed by the determination of a series of physically meaningful quantities including normal stress, SIFs, and net force.

3. Numerical implementation

For the convenience of numerical analysis, it would be better to rewrite Eqs. (11a) and (11b) into dimensionless forms first. Simple dimensional analysis on Eqs. (10a) and (11a) indicates that the unknown function $F_1^*(s)$ in Eq. (13a) carries the same dimension as $E^*\delta$. We therefore

introduce following dimensionless quantities $\bar{u} \equiv \frac{u}{a}$, $\bar{s} \equiv \frac{s}{a}$, $c \equiv \frac{a}{b}$, $\bar{F}_1^*(\bar{s}) \equiv \frac{F_1^*(s)}{E^*\delta}$. Eqs. (11a) and (11b) thus can be normalized to be

$$\bar{F}_1^*(\bar{s}) + \frac{2}{\pi^2}\int_0^1 \bar{Q}_1(\bar{u},\bar{s})\bar{F}_1^*(\bar{u})d\bar{u} = \bar{g}(\bar{s}), \quad (0 \le \bar{s} \le 1) \tag{16a}$$

where

$$\bar{Q}_1(\bar{u},\bar{s}) \equiv aQ_1(u,s) = \left(\bar{u}\ln\frac{1+\bar{s}c}{1-\bar{s}c} - \bar{s}\ln\frac{1+\bar{u}c}{1-\bar{u}c}\right)\frac{1}{\left(\bar{u}^2-\bar{s}^2\right)}, \quad (0 \le \bar{u} \le 1,\ \ 0 \le \bar{s} \le 1) \tag{16b}$$

$$\bar{g}(\bar{s}) \equiv \frac{1}{2\pi}\ln\frac{1-\bar{s}c}{1+\bar{s}c}, \ (0 \le \bar{s} \le 1) \tag{16c}$$

Fig. 2 plots the normalized kernel function $\bar{Q}_1(\bar{u},\bar{s})$ in the domain of $0 \le \bar{u},\bar{s} \le 1.0$ for selected values of $c = 0.25, 0.5, 0.75$, and 1.0. When c is much smaller than 1.0, function $\bar{Q}_1$ is vanishingly small. This behaviour of $\bar{Q}_1$, which can also be inferred from Eq. (16b), implies an asymptotical solution to Eq. (16a) when $c \to 0$. That is, $\bar{F}_1^*(\bar{s}, c \to 0) \cong \bar{g}(\bar{s}) \equiv \frac{1}{2\pi}\ln\frac{1-\bar{s}c}{1+\bar{s}c}$. Therefore, function $\bar{g}(\bar{s})$ can be deemed as an approximate analytical solution to $\bar{F}_1^*(\bar{s})$ for $c \ll 1.0$. In another limit of $c \to 1.0$, function $\bar{Q}_1$ is vanishingly small in most of the domain but exhibits considerable value near the singular point at $\bar{u} = \bar{s} = 1.0$. Finding the asymptotical solution in the limit of $c \to 1.0$ remains a challenge.

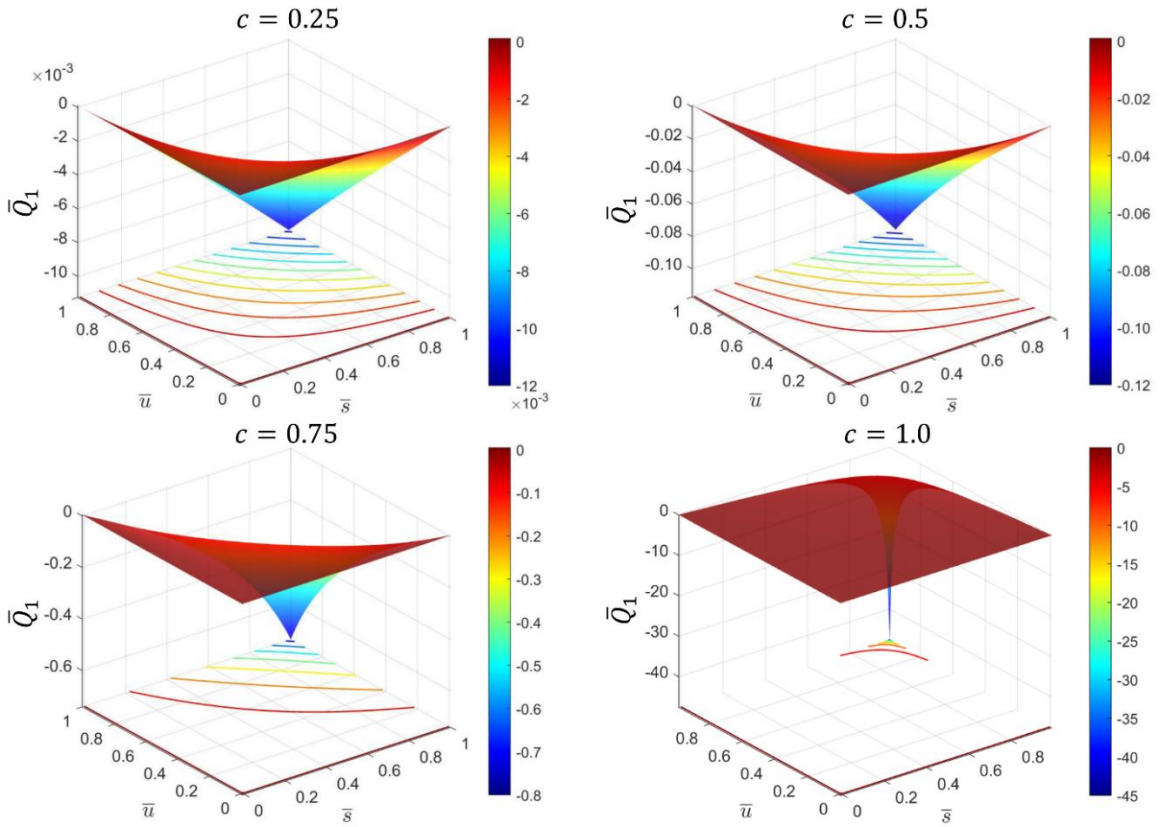

Fig. 2. Plots the dimensionless kernel function $\bar{Q}_1(\bar{u},\bar{s})$ in the domain of $0 \le \bar{u},\bar{s} \le 1.0$ for $c = 0.25, 0.5, 0.75, 1.0$, respectively.

Substitution of variable $x \equiv 2\bar{u} - 1$ in Eq. (16a) converts the integral interval into the standard form $[-1, 1]$ for *Gauss-Lobatto* quadrature (Kovvali, 2013). Eq. (16a) thus is rewritten as

$$\bar{F}_1^*(\bar{s}) + \frac{1}{\pi^2}\int_{-1}^{1} \bar{Q}_1\left(\tfrac{x+1}{2}, \bar{s}\right)\bar{F}_1^*(\tfrac{x+1}{2})dx = \bar{g}(\bar{s}),\ (\bar{s} \le 1) \tag{17}$$

Applying the *Gauss-Lobatto* quadrature to Eq. (17) gives

$$\bar{F}_1^*(\bar{s}) + \frac{1}{\pi^2}\sum_{j=1}^{n} w_j \bar{Q}_1\left(\tfrac{x_j+1}{2}, \bar{s}\right)\bar{F}_1^*(\tfrac{x_j+1}{2}) = \bar{g}(\bar{s}) \tag{18}$$

where n is the number of integration points, $x_j\ (j = 1, \cdots, n)$ are the integration points including the endpoints $x_1 = -1$ and $x_n = 1$, and $w_j\ (j = 1, \cdots, n)$ are the corresponding weights with $w_1 = w_n = \frac{2}{n(n-1)}$. In Eq. (18), taking $\bar{s}$ as values of $\bar{s}_i = \frac{x_i+1}{2}\ (i = 1, \cdots, n)$, we obtain n equations about n unknowns $\bar{F}_1^*\left(\frac{x_i+1}{2}\right)(i = 1, \cdots, n)$. These equations can be written in a matrix form as follows:

$$(\mathbf{I} + \frac{1}{\pi^2}\mathbf{K})\bar{\mathbf{F}}_1^* = \bar{\mathbf{g}} \tag{19}$$

where $\mathbf{I}$ is the $n \times n$ unit matrix and

$$\mathbf{K} = \begin{bmatrix} \frac{2\bar{Q}_1(0,0)}{n(n-1)} & \cdots & w_j\bar{Q}_1\left(\frac{x_j+1}{2}, 0\right) & \cdots & \frac{2\bar{Q}_1(1,0)}{n(n-1)} \\ \vdots & \vdots & \vdots & \vdots & \vdots \\ \frac{2\bar{Q}_1\left(0, \frac{x_i+1}{2}\right)}{n(n-1)} & \cdots & w_j\bar{Q}_1\left(\frac{x_j+1}{2}, \frac{x_i+1}{2}\right) & \cdots & \frac{2\bar{Q}_1\left(1, \frac{x_i+1}{2}\right)}{n(n-1)} \\ \vdots & \vdots & \vdots & \vdots & \vdots \\ \frac{2\bar{Q}_1(0,1)}{n(n-1)} & \cdots & w_j\bar{Q}_1\left(\frac{x_j+1}{2}, 1\right) & \cdots & \frac{2\bar{Q}_1(1,1)}{n(n-1)} \end{bmatrix}_{n\times n,} \quad \bar{\mathbf{F}}_1^* = \begin{bmatrix} \bar{F}_1^*(0) \\ \vdots \\ \bar{F}_1^*(\frac{x_j+1}{2}) \\ \vdots \\ \bar{F}_1^*(1) \end{bmatrix}_{n\times 1,} \quad \bar{\mathbf{g}} = \begin{bmatrix} \bar{g}(0) \\ \vdots \\ \bar{g}(\frac{x_i+1}{2}) \\ \vdots \\ \bar{g}(1) \end{bmatrix}_{n\times 1}$$

Solving Eq. (19) for the unknown array $\bar{\mathbf{F}}_1^*$ by left multiplying the inverse matrix of $(\mathbf{I} + \frac{1}{\pi^2}\mathbf{K})$ on both sides gives rise to

$$\bar{\mathbf{F}}_1^* = (\mathbf{I} + \frac{1}{\pi^2}\mathbf{K})^{-1}\bar{\mathbf{g}} \tag{20}$$

Eq. (20) gives the numerical solution to the function $\bar{F}_1^*(\bar{s})$ at all the integration points including $\bar{s}_1 = 0$ and $\bar{s}_n = 1$.

On the other hand, we introduce dimensionless quantities $\bar{u} \equiv \frac{u}{a}$, $\bar{s} \equiv \frac{s}{b}$, $\bar{F}_2^*(\bar{s}) \equiv \frac{F_2^*(s)}{E^*\delta}$ into Eq. (10b) to rewrite it into a normalized form as

$$\bar{F}_2^*\left(\bar{s}\right) = -\frac{2c^2}{\pi}\int_0^1 \frac{\bar{u}\bar{F}_1^*\left(\bar{u}\right)d\bar{u}}{\left(\bar{s}^2 - \bar{u}^2c^2\right)} + \frac{1}{2},\ \left(1 \le \bar{s} < \infty\right) \tag{21}$$

For $c \ll 1.0$, substituting the asymptotic solution $\bar{F}_1^*(\bar{u}, c \to 0) \cong \frac{1}{2\pi}\ln\frac{1-\bar{u}c}{1+\bar{u}c} \cong -\frac{\bar{u}c}{\pi}$ into Eq. (21), we obtain the asymptotic solution $\bar{F}_2^*(\bar{s}, c \to 0) \cong \frac{2c}{\pi^2}\left[\frac{\bar{s}}{2c}\ln\frac{\bar{s}+c}{\bar{s}-c} - 1\right] + \frac{1}{2}$. For a general c, applying *Gauss-Lobatto* quadrature and the numerical solution to $\bar{F}_1^*$ above to Eq. (21), we have the numerical solution to $\bar{F}_2^*(\bar{s})$ as

$$\bar{F}_2^*\left(\bar{s}\right) = -\frac{c^2}{\pi}\sum_{j=1}^{n} w_j \bar{Q}_2\left(\frac{x_j+1}{2}, \bar{s}\right)\bar{F}_1^*\left(\frac{x_j+1}{2}\right) + \frac{1}{2} \tag{22}$$

where $\bar{Q}_2\left(\frac{x_j+1}{2}, \bar{s}\right) \equiv \frac{(x_j+1)/2}{[\bar{s}^2-(x+1)^2c^2/4]}$, n is the number of integration points, x_j $(j = 1, \cdots, n)$ are the integration points including the endpoints $x_1 = -1$ and $x_n = 1$, and w_j are the corresponding weights with $w_1 = w_n = \frac{2}{n(n-1)}$.

The normalized stress in the ligament (bonded) region $(c < \bar{r} < 1)$, according to Eq. (13a), is given by

$$\bar{\sigma}_{zz}\left(\bar{r}\right) \equiv \frac{\sigma_{zz}\left(r\right)b}{E^*\delta},\ \left(c < \bar{r} < 1\right)$$

$$= \frac{4}{\pi^2}\left[-\arctan\left(\frac{1-\bar{r}^2}{\bar{r}^2-c^2}\right)^{1/2}\frac{\bar{F}_1^*\left(1\right)}{\left(\bar{r}^2-c^2\right)^{1/2}} + \frac{\pi\bar{F}_2^*\left(1\right)}{2\left(1-\bar{r}^2\right)^{1/2}} + \int_0^1 \bar{F}_1^{*\prime}\left(\bar{u}\right)\bar{Q}_3\left(\bar{r}, \bar{u}, c\right)d\bar{u}\right] \tag{23a}$$

where

$$\bar{Q}_3\left(\bar{r}, \bar{u}, c\right) = \left(\bar{r}^2 - \bar{u}^2c^2\right)^{-1/2}\arctan\left(\frac{1-\bar{r}^2}{\bar{r}^2-\bar{u}^2c^2}\right)^{1/2} \tag{23b}$$

Applying *Gauss-Lobatto* quadrature to calculate the integral in Eq. (23a), we have the numerical solution to the normal stress as

$$\bar{\sigma}_{zz}\left(\bar{r}\right) = \frac{4}{\pi^2}\left[-\arctan\left(\frac{1-\bar{r}^2}{\bar{r}^2-c^2}\right)^{1/2}\frac{\bar{F}_1^*\left(1\right)}{\left(\bar{r}^2-c^2\right)^{1/2}} + \frac{\pi\bar{F}_2^*\left(1\right)}{2\left(1-\bar{r}^2\right)^{1/2}} + \frac{1}{2}\sum_{j=1}^{n} w_j\bar{F}_1^{*\prime}\left(\bar{u}_j\right)\bar{Q}_3\left(\bar{r}, \bar{u}_j, c\right)\right] \tag{23c}$$

where n is the number of integration points, $\bar{u}_j = \frac{x_j+1}{2}$ with x_j $(j = 1, \cdots, n)$ being the integration points including the endpoints $x_1 = -1$ and $x_n = 1$, and w_j $(j = 1, \cdots, n)$ are the corresponding weights with $w_1 = w_n = \frac{2}{n(n-1)}$.

The normalized SIFs at the PSC tip (point A) and the ECC tip (point B), according to Eqs. (14a) and (14b), are given by

$$\bar{K}_{\mathrm{A}} \equiv \frac{K_{\mathrm{A}}\sqrt{b\pi}}{E^*\delta} = -\frac{2\bar{F}_1^*(1)}{\sqrt{c}} \tag{24a}$$

$$\bar{K}_{\mathrm{B}} \equiv \frac{K_{\mathrm{B}}\sqrt{b\pi}}{E^*\delta} = 2\bar{F}_2^*(1) \tag{24b}$$

Their asymptotic solutions for $c \to 0$ are given by

$$\bar{K}_{\mathrm{A}}(c \to 0) \cong \frac{1}{\pi\sqrt{c}} \ln\frac{1+c}{1-c} \tag{24c}$$

$$\bar{K}_{\mathrm{B}}(c \to 0) \cong \frac{4c}{\pi^2}\left[\frac{1}{2c}\ln\frac{1+c}{1-c} - 1\right] + 1 \tag{24d}$$

The normalized net force, according to Eq. (15), is given by

$$\bar{P}(c) \equiv \frac{P}{bE^*\delta} = 2\left(1-c^2\right)^{1/2} - \frac{8c}{\pi}\int_0^1 \frac{\bar{Q}_4(\bar{u},c)}{\left(1-\bar{u}^2\right)^{1/2}}\bar{F}_1^*(\bar{u})\,d\bar{u} \tag{25a}$$

where

$$\bar{Q}_4(\bar{u},c) = \bar{u}\arctan\left(\frac{1-c^2}{c^2-c^2\bar{u}^2}\right)^{1/2} \tag{25b}$$

Since the integrand in Eq. (25a) contains $(1-\bar{u}^2)^{-\frac{1}{2}}$ which is singular at the endpoint of interval $\bar{u} = 1$, *Gauss-Chebyshev* quadrature is applied, which gives rise to

$$\int_0^1 \frac{\bar{Q}_4(\bar{u},c)}{\left(1-\bar{u}^2\right)^{1/2}}\bar{F}_1^*(\bar{u})\,d\bar{u} = \sum_{j=1}^{n/2}\bar{Q}_4(\bar{u}_j,c)\bar{F}_1^*(\bar{u}_j)w_j \tag{26}$$

where n is the number of integration points, integration points $\bar{u}_j = \cos\left(\frac{2j-1}{2n}\pi\right)$, and weights $w_j = \frac{\pi}{n}$. Different from the standard *Gauss-Chebyshev* quadrature formula, here the index of summation is taken from $j = 1$ to $n/2$ because the integration interval in Eq. (25a) is $[0, 1]$ which is half of the standard interval $[-1, 1]$ of the *Gauss-Chebyshev* quadrature.

4. Results and discussion

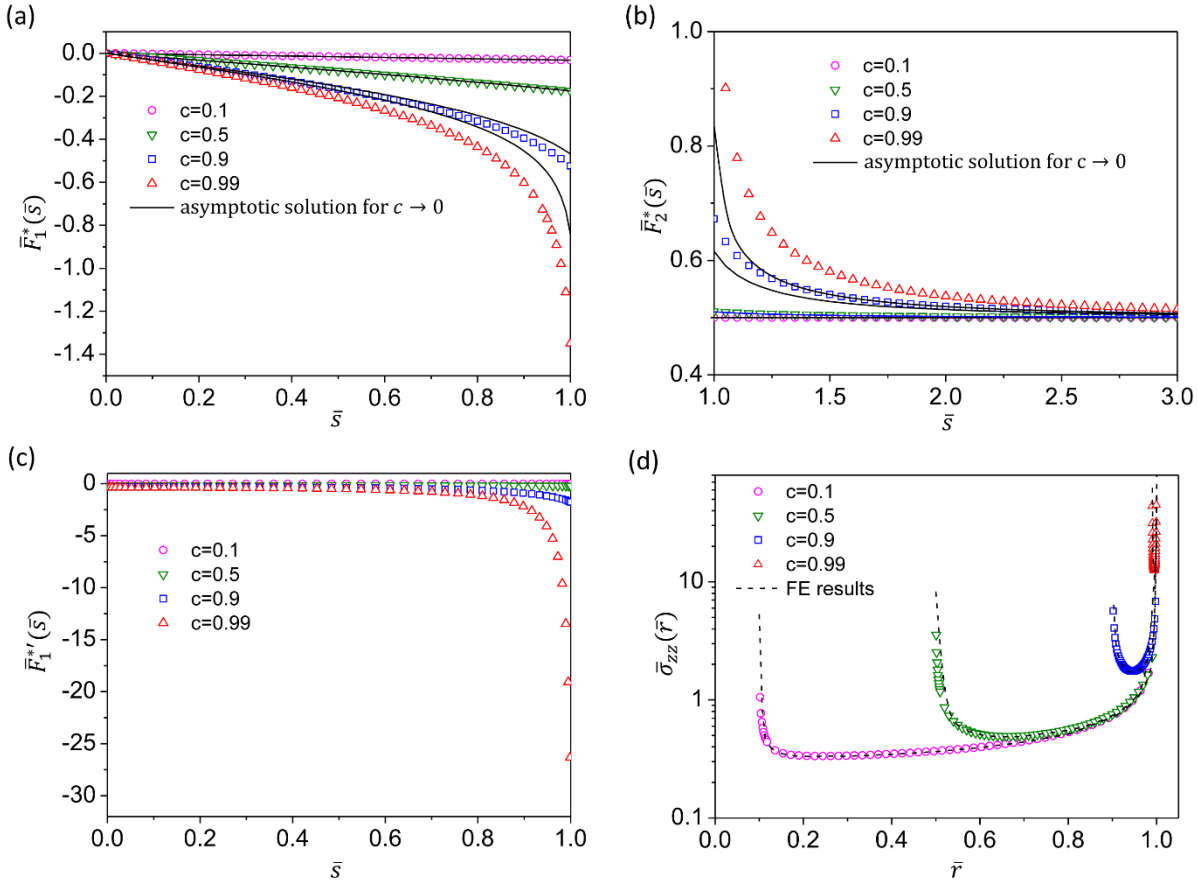

Fig. 3. Numerical solutions to functions (a) $\bar{F}_1^*(\bar{s})$, (b) $\bar{F}_2^*(\bar{s})$, (c) $\bar{F}_1^{*\prime}(\bar{s})$ and (d) normal stress $\bar{\sigma}_{zz}(\bar{r})$ for selected values of c. The solid lines in (a) and (b) plot the asymptotic solutions $\bar{F}_1^*(\bar{s}, c \to 0) \cong \frac{1}{2\pi}\ln\frac{1-\bar{s}c}{1+\bar{s}c}$ and $\bar{F}_2^*(\bar{s}, c \to 0) \cong \frac{2c}{\pi^2}\left[\frac{\bar{s}}{2c}\ln\frac{\bar{s}+c}{\bar{s}-c} - 1\right] + \frac{1}{2}$ respectively for selected $c = 0.1, 0.5, 0.9,$ and 0.99.

The numerical algorithm constructed above is implemented with MATLAB scripts (R2015a, The MathWorks Inc.), in which 50 integration points were adopted in the *Gauss-Lobatto* quadrature in Eqs. (18), (22) and (23c) and the *Gauss-Chebyshev* quadrature in Eq. (26). Fig. 3a shows our numerical solutions to $\bar{F}_1^*(\bar{s})$ for selected value of $c = 0.1, 0.5, 0.9,$ and 0.99. For comparison, here we also plot the asymptotic solution $\bar{F}_1^*(\bar{s}, c \to 0) \cong \frac{1}{2\pi}\ln\frac{1-\bar{s}c}{1+\bar{s}c}$ as the approximate solution to $\bar{F}_1^*(\bar{s})$ for the c selected above. When $c \ll 1.0$, the asymptotic solution perfectly fits the numerical solution to $\bar{F}_1^*(\bar{s})$. Even at $c = 0.7$, the maximum discrepancy between the asymptotic solution and numerical solution, which occurs at $\bar{s} = 1.0$, remains less than 3%. As c increases further and approaches 1.0, the discrepancy between them increases. The maximum difference between them reaches about 10% when $c = 0.9$ and 37.6% when $c = 0.99$. Based on the obtained numerical solution to $\bar{F}_1^*(\bar{s})$, Eq. (22) then is applied to

calculate the numerical solution to $\bar{F}_2^*(\bar{s})$. Fig. 3b shows our numerical solutions to $\bar{F}_2^*(\bar{s})$ for selected $c = 0.1, 0.5, 0.9$, and 0.99 in comparison with the asymptotic solution $\bar{F}_2^*(\bar{s}, c \to 0) \cong \frac{2c}{\pi^2}\left[\frac{\bar{s}}{2c}\ln\frac{\bar{s}+c}{\bar{s}-c} - 1\right] + \frac{1}{2}$. Likewise, when $c \ll 1.0$, this asymptotic solution perfectly depicts the solution to $\bar{F}_2^*(\bar{s})$ very well. Large discrepancy can be observed when c increases and approaches 1.0.

Based on the obtained numerical solution to $\bar{F}_1^*(\bar{s})$, we further calculate its derivative $\bar{F}_1^{*\prime}(\bar{s})$ simply by approximating it as the linear slope between two adjacent points on the $\bar{F}_1^*(\bar{s})$ curve. The result is shown in Fig. 3c. Then, the normalized stress $\bar{\sigma}_{zz}(\bar{r})$ in the ligament (bonded) region ($c < \bar{r} < 1$) is calculated based on the obtained $\bar{F}_1^{*\prime}(\bar{s})$ using Eq. (23c). Fig. 3d shows the normalized stress $\bar{\sigma}_{zz}(\bar{r})$ for $c = 0.1, 0.5, 0.9$, and 0.99, which shows good agreement with the FE results (ABAQUS, Dassault Systèmes). As expected, the stress exhibits singularity of different extents near the crack tips ($\bar{r} = c, \bar{r} = 1$). However, the stress distribution is not symmetric when c is relatively small. In particular, the stress near the ECC ($\bar{r} = 1$) is higher than that near the PSC ($\bar{r} = c$). As the size of the ligament (bonded) region is reduced, c increases and approaches 1.0. The stress becomes more symmetric, resulting in a U-shaped distribution.

From the numerical solutions to $\bar{F}_1^*(\bar{s})$ and $\bar{F}_2^*(\bar{s})$ obtained above, the normalized SIFs at both crack tips can be obtained through Eqs. (26a) and (26b). Fig. 4a shows the calculated $\bar{K}_{\mathrm{A}}$ and $\bar{K}_{\mathrm{B}}$ in comparison with those computed by the finite element (FE) method (ABAQUS, Dassault Systèmes). Our numerical quadrature-based results agree perfectly well with the FE results in the whole spectrum of $c \in (0,1)$. Meanwhile, our results indicate that $\bar{K}_{\mathrm{A}}$ and $\bar{K}_{\mathrm{B}}$ can be nicely approximated by the asymptotic solutions $\bar{K}_{\mathrm{A}}(c \to 0) \cong \frac{1}{\pi\sqrt{c}}\ln\frac{1+c}{1-c}$ and $\bar{K}_{\mathrm{B}}(c \to 0) \cong \frac{4c}{\pi^2}\left[\frac{1}{2c}\ln\frac{1+c}{1-c} - 1\right] + 1$ when $c < 0.7$. In particular, when $c = 0$ our numerical solution to $\bar{K}_{\mathrm{B}}$ is successfully reduced to the SIF of a single externally circular crack, which is analytically given by $K = E^*\delta/\sqrt{b\pi}$ (Tada et al., 2000). The SIF at the ECC tip ($\bar{K}_{\mathrm{B}}$) varies little in the range of $0 < c < 0.5$, implying that the interior PSC affects little on the exterior ECC when the $a/b < 0.5$. With the increase of c, especially when $c > 0.8$, both SIFs grow quickly with c and approach infinity as $c \to 1.0$. Such a singularity of the SIFs at $c \to 1$ is essentially attributed to the vanishing size of the ligament (contact) region and therefore the infinite average stress. From Fig. 4a, one can see that for a combo crack under remote tensile load, the SIF at the exterior ECC tip ($\bar{K}_{\mathrm{B}}$) is always higher than that at the interior PSC tip ($\bar{K}_{\mathrm{A}}$). But the difference between them decreases as the size of the contact region is reduced (i.e., $c \to 1$). This behaviour

is consistent with the variation of stress distribution with c as shown in Fig. 3d. The normalized net force calculated from Eq. (25a) is shown in Fig. 4b as a function of c in comparison with the FE results. Again, our numerical quadrature-based result of the force load agrees faithfully with the FE result and is successfully reduced to the analytical solution to the single externally circular crack (i.e., $P = 2bE^*\delta$) when $c = 0$.

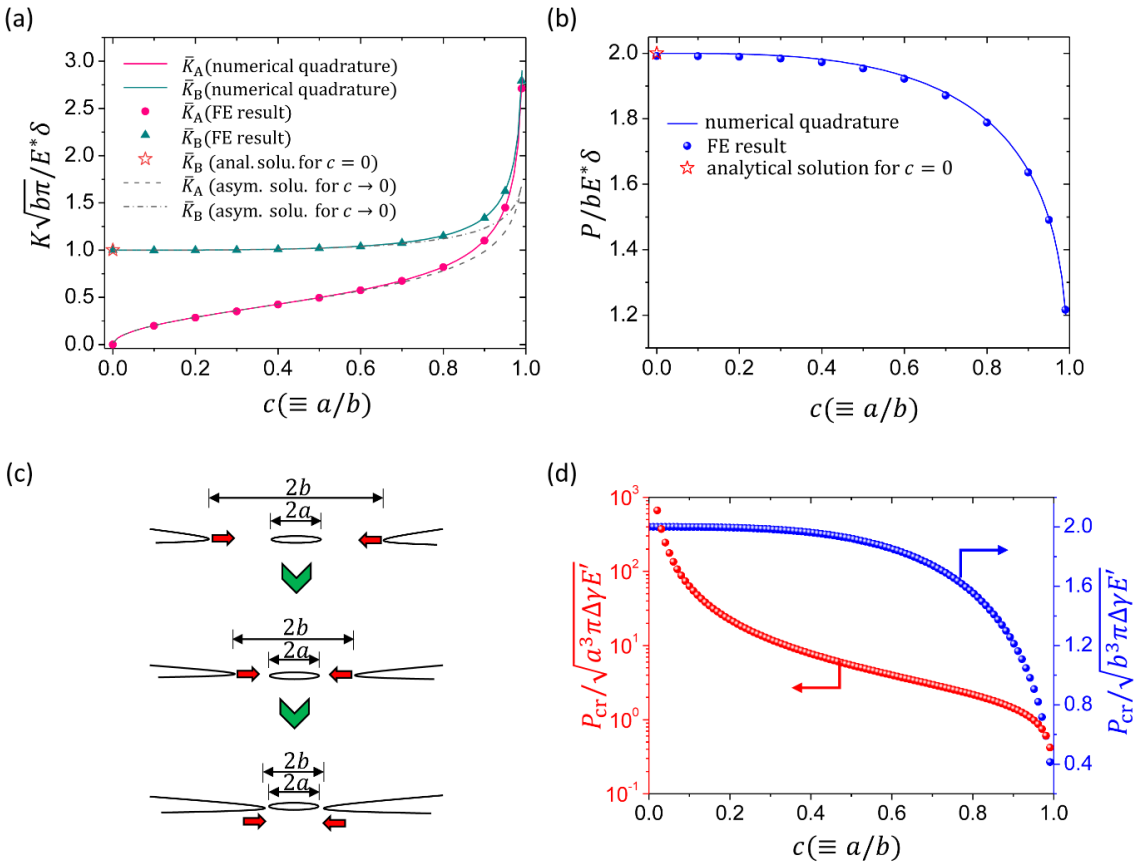

Fig. 4. (a) Numerical quadrature-based solutions to the normalized SIFs at the PSC tip ($\bar{K}_A$) and the ECC tip ($\bar{K}_B$) in comparison to the FE results. The hollow star symbol represents the analytical solution $\bar{K}_B = 1.0$ when $c = 0$ (Tada et al., 2000). The asymptotic solutions $\bar{K}_A \cong \frac{1}{\pi\sqrt{c}}\ln\frac{1+c}{1-c}$ and $\bar{K}_B \cong \frac{4c}{\pi^2}\left[\frac{1}{2c}\ln\frac{1+c}{1-c} - 1\right] + 1$ for $c \to 0$ are plotted with dash line and dash-dot line respectively. (b) The numerical quadrature-based solution to the normalized net force as a function of c in comparison to the FE result. The hollow star symbol represents the analytical solutions $P = 2bE^*\delta$ when $c = 0$ (Tada et al., 2000). (c) Schematic snapshots of the crack propagation process of a combo crack under remote tensile load. (d) Critical tensile force for crack propagation normalized by $\sqrt{a^3\pi\Delta\gamma E'}$ (the left y-axis) and $\sqrt{b^3\pi\Delta\gamma E'}$ (the right y-axis) respectively.

The acquisition of the SIFs and the net force for a given load δ allows us to determine the critical force load at which crack propagation happens. Since the SIF at the ECC tip is always higher than that at the PSC tip irrespective of the value of c (Fig. 4a), when a combo crack is subjected to a sufficient remote force load, inward crack propagation will occur always at the

ECC while the interior PSC is pinned, as schematically shown in Fig. 4c. Classical Griffith's criterion for crack propagation (Griffith, 1921) indicates that crack will propagate when the SIF reaches a critical value of $K_c \equiv \sqrt{E'\Delta\gamma}$, where $E' = E^*$ for a crack problem (see Fig. 1a) and $E' = 2E^*$ for a contact problem (see Fig. 1b), and $\Delta\gamma$ is the fracture energy for a crack problem or work of adhesion for a contact problem (Israelachvili, 1992). By equating K_B with $\sqrt{E'\Delta\gamma}$ and replacing δ with force load P, we determine the critical force load corresponding to crack propagation as $P_{cr} = \frac{\sqrt{b^3\pi\Delta\gamma E'}\bar{P}}{\bar{K}_B}$, where $\bar{K}_B$ and $\bar{P}$ as functions of c have been shown in Fig. 4a and Fig. 4b, respectively. Fig. 4d plots the P_{cr} normalized by $\sqrt{a^3\pi\Delta\gamma E'}$ and $\sqrt{b^3\pi\Delta\gamma E'}$ as a function of c. The critical force load decreases monotonically with increasing c (or decreasing b), implying that the propagation of the ECC under remote force load is an unstable process. Once it is triggered, it would proceed spontaneously until the catastrophic fracture of the material or the adhesion. This is distinct from the cracking behaviour of a combo crack under pressure load applied to the PSC surface, when cracking of the PSC is a stable process until the critical pressure load reaches its maximum value (Yao and Zhang, 2022). The quantitative solutions to the normalized SIFs, force load, and critical load for crack propagation are tabulated in Table 1 for selected values of c ranging from 0 to 0.999. To make an easy comparison with the previous SIF results reported in the literatures (Murakami, 1992; Yong and Hanson, 1994), here we also present our SIFs by using their normalization scheme, as shown in the last two rows in Table 1. In comparison with their results, our SIFs exhibit much higher precision. For example, in the limiting case of $c = 0$ our result of $\frac{2K_A b^2\sqrt{\pi}}{P\sqrt{a}}$ is 0.6366, which is closer to the analytical solution $2/\pi$ than their result (0.634). Moreover, the accuracy of our results is ensured for any c less than 1.0.

Table 1. Normalized stress intensity factors and loads for selected values of *a/b*

$c \equiv a/b$	0	0.1	0.2	0.3	0.4	0.5	0.6	0.7	0.8	0.9	0.99	0.999
$\frac{K_A\sqrt{b\pi}}{E^*\delta}$	0	0.2020	0.2887	0.3602	0.4279	0.4981	0.5777	0.6776	0.8228	1.1046	2.7120	6.7659
$\frac{K_B\sqrt{b\pi}}{E^*\delta}$	1.0000	1.0001	1.0011	1.0039	1.0100	1.0213	1.0417	1.0791	1.1537	1.3451	2.7960	6.8380
$\frac{P}{bE^*\delta}$	2.0000	1.9997	1.9978	1.9924	1.9814	1.9620	1.9301	1.8790	1.7952	1.6420	1.2165	0.9432
$\frac{P_{cr}}{\sqrt{b^3\pi\Delta\gamma E'}}$	2.0000	1.9995	1.9956	1.9847	1.9618	1.9211	1.8528	1.7413	1.5560	1.2207	0.4351	0.1379
$\frac{2K_A b^2\sqrt{\pi}}{P\sqrt{a}}$ §	0.6366	0.6389	0.6463	0.6601	0.6829	0.7181	0.7728	0.8620	1.0249	1.4182	4.4812	14.354
$\frac{2K_B b^2\sqrt{\pi}}{P\sqrt{b}}$ §	1.0000	1.0003	1.0022	1.0077	1.0195	1.0411	1.0794	1.1486	1.2853	1.6384	4.5968	14.500

[§]The normalization scheme here follows that in a published handbook (Murakami, 1992). However, in their stress intensity factors a factor of $\sqrt{\pi}$ was missing, which actually resulted from the deficiency of this factor in the equations (49)(50) in the original paper (Yong and Hanson, 1994).

For a combo crack, our discussion above manifested that remote force load always causes inward crack propagation of the ECC, whereas our earlier study in Part I (Yao and Zhang, 2022) indicated that pressure load on the PSC surface always results in outward crack propagation of the PSC. How would a combo crack propagate upon a pressure load on the PSC surface in combination with a remote force load? To answer this question, we consider a combo crack subjected to a pre-loaded pressure p_{in} on the PSC surface and a varying force P at distance, as schematically illustrated in Fig. 5a. Based on the result shown in Fig. 4 and that reported in Part I (Yao and Zhang, 2022), the SIFs at the tips of the PSC (point A) and ECC (point B) due to such combined load are calculated by superposition. Equating the calculated SIFs at points A and B with the critical stress intensity factor for crack propagation $K_{\text{c}} \equiv \sqrt{E'\Delta\gamma}$ (Griffith, 1921), we determine the critical force load required to trigger the propagation at the PSC or ECC respectively, which are denoted by P_{cr}^{A} and P_{cr}^{B}. The crack with lower critical force load for propagation will grow preferably. Fig. 5b compares the normalized P_{cr}^{A} and P_{cr}^{B} as functions of c for a selected pre-loaded pressure p_{in}. When $c \ll 1$, P_{cr}^{B} is smaller than P_{cr}^{A}, implying that inwards crack propagation happens preferably at the ECC while the PSC then is pinned (a is kept constant). In contrast, when c exceeds a threshold $c_{\text{th}} \approx 0.42$, P_{cr}^{B} surpasses P_{cr}^{A}, implying that outwards crack propagation happens preferably at the PSC while the ECC then is pinned (b is kept constant). Such a switch of the cracking direction in the fracture process is schematically shown in Fig. 5c. To manifest the genuine variations of the critical force loads with c, in Fig. 5b P_{cr}^{A} and P_{cr}^{B} are normalized by constant $\sqrt{a^3\pi\Delta\gamma E'}$ for $c < 0.42$ and constant $\sqrt{b^3\pi\Delta\gamma E'}$ for $c > 0.42$. In the whole spectrum of c, the critical force load decreases monotonically as c increases, implying that the pre-loaded inner pressure does not affect the instability of the fracture process of a combo crack system under remote force load. In Fig. 5b, the pre-loaded pressure is taken as $p_{\text{in}} = 0.5\sqrt{\Delta\gamma E'/a}$. Further studies with different pre-loaded pressure p_{in} indicate that the threshold c_{th}, at which crack propagation switches from the ECC to PSC, depends on the pre-loaded pressure p_{in}. The higher the p_{in}, the lower the c_{th}. If $p_{\text{in}} = 0.7\sqrt{\Delta\gamma E'/a}$, for example, c_{th} will be reduced to ~0.11. An excessive pre-loaded p_{in} might completely suppress the occurrence of the propagation of the ECC, leaving unidirectional cracking at the PSC only.

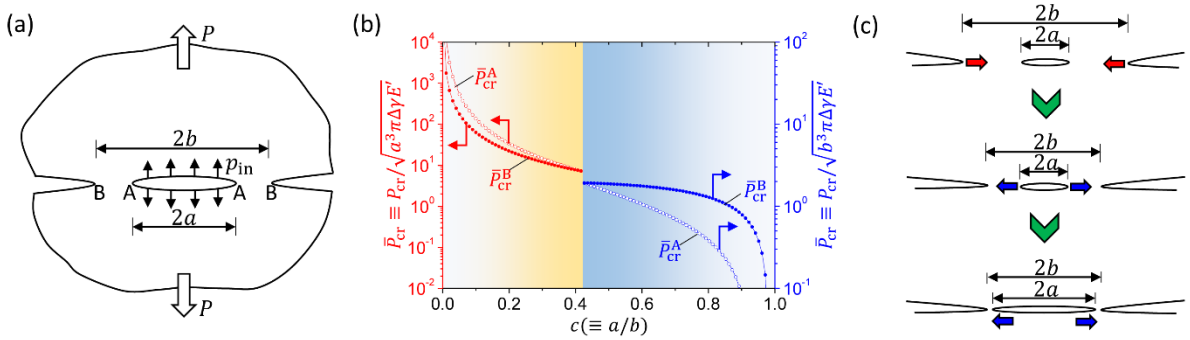

Fig. 5. (a) Cross-sectional illustration of a combo crack subjected to a pre-loaded inner pressure p_{in} on the PSC surface and force load P at distance. (b) Variations of the normalized critical remote force loads $\bar{P}_{\text{cr}}^{\text{A}}$ and $\bar{P}_{\text{cr}}^{\text{B}}$ with c for a given pre-loaded inner pressure $p_{\text{in}} = 0.5\sqrt{\Delta\gamma E'/a}$ $(c < 0.42)$ or equivalently $p_{\text{in}} = 0.77\sqrt{\Delta\gamma E'/b}$ $(c > 0.42)$. (c) Schematics showing the transition of the cracking direction in a combo crack under an appropriate pre-loaded pressure on the PSC surface and remote force load.

5. Conclusion

To make up for the lack of a reliable and high-precision solution to the combo-crack problem under remote load, in this paper we revisited this classical problem in fracture mechanics. Based on the Hankel transform-based representations of the general solution to axisymmetric elasticity problems, we formulated the concerned triple mixed boundary problem into a pair of simultaneous Fredholm integral equations about two unknown functions. Then, we merged two integral equations into a single inhomogeneous Fredholm integral equation about one unknown function. *Gauss-Lobatto* quadrature was applied to solve the unknown function numerically, whereby a series of physically meaningful quantities were determined including the normal stress distribution, SIFs, net force, critical load for crack propagation. Our results were verified with the FE results and exhibited higher precision in comparison with the previous power series-based results in literatures. The present solution for the remote load in combination with that for the pressure load on the PSC surface reported earlier (Yao and Zhang, 2022) enabled us to unveil the phenomenon of transition of cracking direction happening in a combo crack under appropriate pre-loaded pressure and remote force load. Our solution, albeit not in closed form, might be the best numerical solution so far to the concerned problem and deserves to be included in the updated handbook for crack problems.

CRediT authorship contribution statement Haimin Yao: Conceptualization, Methodology, Formal analysis, Visualization, Writing – original draft, Supervision. **Chong Zhang:** Validation, Writing – review & editing.

Declaration of Competing Interest

The authors declare that they have no known competing financial interests or personal relationships that could have appeared to influence the work reported in this paper.

Acknowledgment

This work was partially supported by the Departmental General Research Fund of The Hong Kong Polytechnic University (G-YBXP). H.Y. thanks Dai Dai for her considerate tending and support during his self-quarantine period in Hong Kong's 5th COVID-19 wave in the spring of 2022.

Appendix A. Derivation of the simultaneous Fredholm integral equations about $F_1(s)$ and $F_2(s)$

Inserting Eq. (5a) into Eq. (6a) to eliminate $f_1(t)$ yields

$$F_1(s)=\frac{d}{ds}\int_s^a \frac{up_1(u)\,du}{\left(u^2-s^2\right)^{1/2}}+\frac{2}{\pi}\frac{d}{ds}\int_s^a\left[\int_b^\infty \frac{tf_2(t)\,dt}{\left(t^2-a^2\right)^{1/2}}\right]\frac{\left(a^2-u^2\right)^{1/2}u\,du}{(t^2-u^2)\left(u^2-s^2\right)^{1/2}},\ (0\le s\le a) \tag{A1}$$

Since $\int_s^a \frac{\left(a^2-u^2\right)^{1/2}u\,du}{(t^2-u^2)\left(u^2-s^2\right)^{1/2}}=\frac{\pi}{2}\left[1-\left(\frac{t^2-a^2}{t^2-s^2}\right)^{1/2}\right]$, Eq. (A1) can be further simplified to be

$$F_1(s)=\frac{d}{ds}\int_s^a \frac{up_1(u)\,du}{\left(u^2-s^2\right)^{1/2}}-s\int_b^\infty \frac{tf_2(t)\,dt}{\left(t^2-s^2\right)^{3/2}},\ (0\le s\le a) \tag{A2}$$

Substituting Eq. (7b) into Eq. (A2) to eliminate $f_2(t)$ gives

$$F_1(s)=\frac{d}{ds}\int_s^a \frac{up_1(u)\,du}{\left(u^2-s^2\right)^{1/2}}-\frac{2}{\pi}s\int_b^\infty\left[\int_b^t \frac{F_2(r)\,dr}{\left(t^2-r^2\right)^{1/2}}\right]\frac{tdt}{\left(t^2-s^2\right)^{3/2}},\ (0\le s\le a)$$

Interchanging the order of integration in the second integral above yields

$$F_1(s)+\frac{2s}{\pi}\int_b^\infty \frac{F_2(u)}{u^2-s^2}\,du=\frac{d}{ds}\int_s^a \frac{rp_1(r)\,dr}{\left(r^2-s^2\right)^{1/2}},\ (0\le s\le a) \tag{A3}$$

In the derivation of Eq. (A3), the relationship $\int_r^\infty \frac{tdt}{\left(t^2-r^2\right)^{1/2}\left(t^2-s^2\right)^{3/2}}=\frac{1}{r^2-s^2}$ has been adopted.

On the other hand, substituting Eq. (5b) into Eq. (6b) to eliminate $f_2(t)$, we have

$$F_2(s)=\frac{d}{ds}\int_b^s \frac{p_2(u)udu}{\left(s^2-u^2\right)^{1/2}}+\frac{2}{\pi}\frac{d}{ds}\int_b^s\left[\int_0^a \frac{uf_1(u)\,du}{\left(b^2-u^2\right)^{1/2}}\right]\frac{\left(t^2-b^2\right)^{1/2}tdt}{\left(t^2-u^2\right)\left(s^2-t^2\right)^{1/2}},\ \left(b\le s<\infty\right) \tag{A4}$$

Since

$$\int_b^s \frac{\left(t^2-b^2\right)^{1/2}tdt}{\left(t^2-u^2\right)\left(s^2-t^2\right)^{1/2}}=\frac{1}{2}\int_{b^2}^{s^2}\frac{\left(x-b^2\right)^{1/2}dx}{\left(x-u^2\right)\left(s^2-x\right)^{1/2}}=\frac{\pi}{2}\left\{1-\left(\frac{b^2-u^2}{s^2-u^2}\right)^{1/2}\right\},\ \left(b\le s<\infty\right)$$

Eq. (A4) can be simplified to be

$$F_2(s)=\frac{d}{ds}\int_b^s \frac{p_2(u)udu}{\left(s^2-u^2\right)^{1/2}}+s\int_0^a \frac{tf_1(t)\,dt}{\left(s^2-t^2\right)^{3/2}},\ \left(b\le s<\infty\right) \tag{A5}$$

Substituting Eq. (7a) into Eq. (A5) to eliminate $f_1(t)$ gives rise to

$$F_2(s)=\frac{d}{ds}\int_b^s \frac{p_2(u)udu}{\left(s^2-u^2\right)^{1/2}}-\frac{2s}{\pi}\int_0^u \frac{tdt}{\left(u^2-t^2\right)^{1/2}\left(s^2-t^2\right)^{3/2}}\int_0^a F_1(u)\,du,\ \left(b\le s<\infty\right)$$

Interchanging the order of integration in the second integral above yields

$$F_2(s)+\frac{2}{\pi}\int_0^a \frac{uF_1(u)\,du}{\left(s^2-u^2\right)}=\frac{d}{ds}\int_b^s \frac{rp_2(r)\,dr}{\left(s^2-r^2\right)^{1/2}},\ \left(b\le s<\infty\right) \tag{A6}$$

In the derivation of Eq. (A6), the relationship $\int_0^u \frac{tdt}{\left(u^2-t^2\right)^{1/2}\left(s^2-t^2\right)^{3/2}}=\frac{u}{s\left(s^2-u^2\right)}$ has been adopted.

Substituting Eq. (5a) and Eq. (5b) into Eq. (A3) and Eq. (A6) respectively to eliminate $p_1(r)$ and $p_2(r)$, we have

459 $$F_1(s)+\frac{2s}{\pi}\int_b^\infty \frac{F_2(u)\,du}{\left(u^2-s^2\right)}=\frac{E^*\delta}{2}\left[\frac{s}{\left(a^2-s^2\right)^{1/2}}-\frac{s}{\left(b^2-s^2\right)^{1/2}}\right],\ (0\le s\le a) \tag{A7}$$

460 $$F_2(s)+\frac{2}{\pi}\int_0^a \frac{uF_1(u)\,du}{\left(s^2-u^2\right)}=\frac{E^*\delta}{2}\left[\frac{s}{\left(s^2-a^2\right)^{1/2}}-\frac{s}{\left(s^2-b^2\right)^{1/2}}\right],(b\le s<\infty) \tag{A8}$$

461

462 **Appendix B. Determination of the normal stress $\sigma_{zz}(r)$ and net force P**

463 Eqs. (1b) and (3) imply that

464 $$H_0\left[\xi^{-2}A(\xi);\ \xi\to r\right]=\int_0^\infty \xi^{-1}A(\xi)J_0(\xi r)\,d\xi=\begin{cases} f_1(r), & (0\le r<a)\\ -\dfrac{E^*\delta}{2}, & (a\le r\le b)\\ f_2(r), & (b<r<\infty)\end{cases} \tag{B1}$$

465 Taking the inverse Hankel transform, which is Hankel transform as well, on both sides of Eq.
466 (B1), we express function $A(\xi)$ in terms of functions $f_1(r)$ and $f_2(r)$ as

467 $$A(\xi)=\xi^2\left[\int_0^a r f_1(r)J_0(\xi r)\,dr-\int_a^b \frac{rE^*\delta}{2}J_0(\xi r)dr+\int_b^\infty r f_2(r)J_0(\xi r)\,dr\right] \tag{B2}$$

468 Substitute Eqs. (7a) and (7b) into Eq. (B2) to replace $f_1(\cdot)$ and $f_2(\cdot)$ with $F_1(\cdot)$ and $F_2(\cdot)$
469 respectively. Function $A(\xi)$ thus is given by

470 $$A(\xi)=\frac{2}{\pi}\xi^2\left[-\int_0^a F_1(s)\left\{\int_0^s \frac{rJ_0(\xi r)\,dr}{(s^2-r^2)^{1/2}}\right\}ds+\int_b^\infty F_2(s)\left\{\int_s^\infty \frac{rJ_0(\xi r)\,dr}{(r^2-s^2)^{1/2}}\right\}ds\right]$$
$$-\frac{E^*\delta}{2}\xi\left[bJ_1(b\xi)-aJ_1(a\xi)\right]$$

471 In the derivation of the above equation, the relationship $\int_a^b rJ_0(\xi r)dr=\xi^{-1}\left[bJ_1(b\xi)-aJ_1(a\xi)\right]$
472 has been adopted. The normal stress in the contact (ligament) region $(a<r<b, z=0)$ then
473 is given by

474 $$\sigma_{zz}(r)=-H_0\left[\xi^{-1}A(\xi);r\right]=-\int_0^\infty A(\xi)J_0(\xi r)d\xi$$

475 $$=-\frac{2}{\pi}\int_0^a \frac{sF_1(s)\,ds}{\left(r^2-s^2\right)^{3/2}}+\frac{2}{\pi}\int_b^\infty \frac{sF_2(s)\,ds}{\left(s^2-r^2\right)^{3/2}}$$

476 $$+\frac{E^*\delta}{2}\int_0^\infty \xi\left[bJ_1(b\xi)-aJ_1(a\xi)\right]J_0(\xi r)d\xi,\ (a<r<b) \tag{B3}$$

477 Since $F_1(s)=\dfrac{E^*\delta}{2}\dfrac{s}{\left(a^2-s^2\right)^{1/2}}+F_1^*(s),\ (0\le s\le a)$, the first integral in Eq. (B3) is given by

478 $$\int_0^a \frac{sF_1(s)ds}{\left(r^2-s^2\right)^{3/2}}=\frac{E^*\delta}{2}\int_0^a \frac{s^2ds}{\left(r^2-s^2\right)^{3/2}\left(a^2-s^2\right)^{1/2}}+\int_0^a \frac{sF_1^*(s)ds}{\left(r^2-s^2\right)^{3/2}},\ (a<r<b)$$

479 The above equation can be further simplified to be (Gradshteyn and Ryzhik, 1994)

480 $$\int_0^a \frac{sF_1(s)ds}{\left(r^2-s^2\right)^{3/2}}=\frac{E^*\delta}{2}\left[\frac{r}{r^2-a^2}\mathbf{E}\left(\frac{a}{r}\right)-\frac{1}{r}\mathbf{K}\left(\frac{a}{r}\right)\right]+\int_0^a \frac{sF_1^*(s)ds}{\left(r^2-s^2\right)^{3/2}},\ (a<r<b) \tag{B4}$$

481 where $\mathbf{K}(\cdot)$ and $\mathbf{E}(\cdot)$ are the complete elliptic integral of the first and second kinds
482 respectively.

483 On the other hand, since $F_2(s)=-\dfrac{E^*\delta}{2}\dfrac{s}{\left(s^2-b^2\right)^{1/2}}+F_2^*(s),\ (b\le s<\infty)$, the second integral

484 in Eq. (B3) is given by

485 $$\int_b^\infty \frac{sF_2(s)ds}{\left(s^2-r^2\right)^{3/2}}=\int_b^\infty \frac{s}{\left(s^2-r^2\right)^{3/2}}\left[-\frac{E^*\delta}{2}\frac{s}{\left(s^2-b^2\right)^{1/2}}+F_2^*(s)\right]ds$$

486 $$=-\frac{E^*\delta}{2}\int_b^\infty \frac{s^2ds}{\left(s^2-r^2\right)^{3/2}\left(s^2-b^2\right)^{1/2}}+\int_b^\infty \frac{sF_2^*(s)}{\left(s^2-r^2\right)^{3/2}}ds,\ (a<r<b)$$

487 The above equation can be further simplified to be (Gradshteyn and Ryzhik, 1994)

488 $$\int_b^\infty \frac{sF_2(s)ds}{\left(s^2-r^2\right)^{3/2}}=\int_b^\infty \frac{sF_2^*(s)ds}{\left(s^2-r^2\right)^{3/2}}-\frac{E^*\delta}{2}\frac{b}{b^2-r^2}\mathbf{E}\left(\frac{r}{b}\right),\ (a<r<b) \tag{B5}$$

489 Moreover, the third integral in Eq. (B3) is given by

490 $$\int_0^\infty \xi\left[bJ_1(b\xi)-aJ_1(a\xi)\right]J_0(\xi r)d\xi,\ (a<r<b)$$

491 $$=\frac{2b\mathbf{E}\left(\frac{r}{b}\right)}{\pi\left(b^2-r^2\right)}+\frac{2}{\pi}\left[\frac{r\mathbf{E}\left(\frac{a}{r}\right)}{\left(r^2-a^2\right)}-\frac{1}{r}\mathbf{K}(a/r)\right],\ (a<r<b) \tag{B6}$$

492 Substituting Eqs. (B4), (B5), and (B6) into Eq. (B3), all the terms with complete elliptic
493 integrals are canceled out by each other. The normal stress is given in terms of functions $F_1^*(s)$
494 and $F_2^*(s)$ as

$$\sigma_{zz}(r,0)=-\frac{2}{\pi}\int_0^a \frac{sF_1^*(s)ds}{\left(r^2-s^2\right)^{3/2}}+\frac{2}{\pi}\int_b^\infty \frac{sF_2^*(s)}{\left(s^2-r^2\right)^{3/2}}ds,\ (a<r<b) \tag{B7}$$

Applying integration by parts in Eq. (B7), we have

$$\sigma_{zz}(r)=\frac{2}{\pi}\left[\frac{-F_1^*(a)}{\left(r^2-a^2\right)^{1/2}}+\int_0^a \frac{F_1^{*\prime}(s)ds}{\left(r^2-s^2\right)^{1/2}}+\frac{F_2^*(b)}{\left(b^2-r^2\right)^{1/2}}+\int_b^\infty \frac{F_2^{*\prime}(s)ds}{\left(s^2-r^2\right)^{1/2}}\right],\ (a<r<b) \tag{B8}$$

where $F_1^{*\prime}(s)$ and $F_2^{*\prime}(s)$ stand for the derivatives of functions $F_1^*(s)$ and $F_2^*(s)$, respectively. Eq.(10b) implies that

$$F_2^{*\prime}(s)=\frac{4s}{\pi}\int_0^a \frac{uF_1^*(u)du}{\left(s^2-u^2\right)^2} \tag{B9}$$

Substituting Eq. (B9) into the second integral in Eq. (B8), we have

$$\sigma_{zz}(r)=\frac{4}{\pi^2}\left[\begin{array}{l}-\arctan\left(\dfrac{b^2-r^2}{r^2-a^2}\right)^{1/2}\dfrac{F_1^*(a)}{\left(r^2-a^2\right)^{1/2}}+\dfrac{\pi F_2^*(b)}{2\left(b^2-r^2\right)^{1/2}}\\ +\displaystyle\int_0^a \frac{F_1^{*\prime}(u)}{\left(r^2-u^2\right)^{1/2}}\arctan\left(\frac{b^2-r^2}{r^2-u^2}\right)^{1/2}du\end{array}\right],\ (a<r<b) \tag{B10}$$

Since $F_2^*(b)$ can be given in terms of $F_1^*(s)$ and $F_1^{*\prime}(s)$ as

$$F_2^*(b)=\frac{E^*\delta}{2}+\frac{1}{\pi}\left[F_1^*(a)\ln\left(b^2-a^2\right)-\int_0^a \ln\left(b^2-u^2\right)F_1^{*\prime}(u)du\right] \tag{B11}$$

Eq. (B10) expresses the normal stress σ_{zz} in terms of $F_1^*(s)$ and its derivative $F_1^{*\prime}(s)$ only.

Moreover, based on the contact stress given by Eq. (B7), the net force can be written as

$$P=2\pi\int_a^b \sigma_{zz}(r,0)rdr=4\int_a^b\left[\int_b^\infty \frac{sF_2^*(s)ds}{\left(s^2-r^2\right)^{3/2}}-\int_0^a \frac{sF_1^*(s)ds}{\left(r^2-s^2\right)^{3/2}}\right]rdr \tag{B12}$$

Interchanging the order of the integration in the double integrals in Eq. (B12), we have

$$P=4\int_b^\infty\left[\frac{s}{\left(s^2-b^2\right)^{1/2}}-\frac{s}{\left(s^2-a^2\right)^{1/2}}\right]F_2^*(s)ds+4\int_0^a\left[\frac{s}{\left(b^2-s^2\right)^{1/2}}-\frac{s}{\left(a^2-s^2\right)^{1/2}}\right]F_1^*(s)ds \tag{B13}$$

Substituting Eq. (10b) into Eq. (B13) to replace $F_2^*(s)$ with $F_1^*(s)$, we have

$$P=2E^*\delta\left(b^2-a^2\right)^{1/2}-\frac{8}{\pi}\int_0^a \arctan\left(\frac{b^2-a^2}{a^2-u^2}\right)^{1/2}\frac{uF_1^*(u)}{\left(a^2-u^2\right)^{1/2}}du \tag{B14}$$